



**Modeling of spin decoherence in a Si hole qubit perturbed by a single charge fluctuator**Baker Shalak  and Christophe Delerue \**Université de Lille, CNRS, Centrale Lille, Université Polytechnique Hauts-de-France, Junia, UMR 8520 - IEMN, F-59000 Lille, France*Yann-Michel Niquet *Université Grenoble Alpes, CEA, IRIG-MEM-L\_Sim, F-38000, Grenoble, France* (Received 20 October 2022; revised 7 March 2023; accepted 9 March 2023; published 20 March 2023)

Spin qubits in semiconductor quantum dots are one of the promising devices to realize a quantum processor. A better knowledge of the noise sources affecting the coherence of such a qubit is therefore of prime importance. In this paper, we study the effect of telegraphic noise induced by the fluctuation of a single electric charge. We simulate as realistically as possible a hole spin qubit in a quantum dot defined electrostatically by a set of gates along a silicon nanowire channel. Calculations combining Poisson and time-dependent Schrödinger equations allow us to simulate the relaxation and the dephasing of the hole spin as a function of time for a classical random telegraph signal. We show that dephasing time  $T_2$  is well given by a two-level model in a wide range of frequencies. Remarkably, in the most realistic configuration of a low-frequency fluctuator, the system has a non-Gaussian behavior in which the phase coherence is lost as soon as the fluctuator has changed state. The Gaussian description becomes valid only beyond a threshold frequency  $\omega_{th}$ , when the two-level system reacts to the statistical distribution of the fluctuator states. We show that the dephasing time  $T_2(\omega_{th})$  at this threshold frequency can be considerably increased by playing on the orientation of the magnetic field and the gate potentials, by running the qubit along “sweet” lines. However,  $T_2(\omega_{th})$  remains bounded due to dephasing induced by the nondiagonal terms of the stochastic perturbation Hamiltonian. On the other hand, our simulations reveal that the spin relaxation, usually characterized by the time  $T_1$ , cannot be described cleanly in the two-level model because the coupling to higher-energy hole levels impacts very strongly the spin decoherence. This result suggests that multilevel simulations including the coupling to phonons should be necessary to describe the relaxation phenomenon in this type of qubit.

DOI: [10.1103/PhysRevB.107.125415](https://doi.org/10.1103/PhysRevB.107.125415)**I. INTRODUCTION**

Spin qubits are being actively studied for quantum computing [1,2]. One path that is being particularly explored at the moment is the use of silicon or germanium qubits [3–10], as it promises extreme miniaturization and integration while benefiting from the expertise and resources of microelectronic technologies. The use of isotopically purified Si substrates also allows one, by suppressing the hyperfine interaction between electrons and nuclear spins, to obtain very long electron spin lifetimes on donors [11] and in quantum boxes defined by electrostatic confinement [12]. This lifetime is particularly long for electrons in conduction band states due to the weak spin-orbit coupling [4], but this makes the manipulation of electron spin via electrical signals not very efficient [13,14].

In this context, hole qubits receive growing interest because of the stronger spin-orbit coupling in the valence band allowing efficient manipulation of the effective spin by electrical means [15–20]. Recent work has demonstrated Rabi oscillations with frequencies of several hundred megahertz in silicon and germanium hole qubits [19–23]. Two-qubit gates have been realized recently [6,9,10,24–26]. In addition,

the strong interaction between spin and microwave photons makes long-distance coupling between qubits possible [27–32]. However, the effective spin-orbit coupling depends on the spatial profile of the hole wave function, lattice deformations, and electric fields, which increases the variability between devices [33] and makes the qubits much more sensitive to phonons and electric potential fluctuations [8,34,35]. It is therefore essential to better understand the influence of these phenomena on the coherence lifetimes of spins in hole qubits in silicon technology. Recent theoretical works have focused on the spin-phonon coupling [36,37]; we are interested here in the influence of charge fluctuations which is usually dominant at low temperature.

Many theoretical studies have investigated the nature and strength of spin-orbit coupling in the heavy hole, light hole, and split-off states of the valence band [17,38]. Proposals have also been made to minimize the effects of electric potential fluctuations [39], to find operating points (the so-called “sweet” spots) where the Larmor frequency becomes insensitive to the fluctuations [40–43]. The considerable increase in the hole spin coherence time at such sweet spots has actually been demonstrated recently in a silicon-on-insulator (SOI) device [44].

Our goal in this paper is different; it is to better understand the physics of hole spin decoherence under the effect of charge

\*christophe.delerue@iemn.fr

fluctuations in a device that is as realistic as possible compared with what was realized experimentally. We consider the case of a hole qubit made on an SOI and formed by electrostatic confinement within a silicon nanowire [19,21]. This qubit is subjected to telegraphic noise due to the fluctuation of a single charge between a metal gate and its neighboring oxide.

The telegraphic noise can be seen as a minimal model reproducing main features of  $1/f$  noise [39,45]. Here we are not interested in the action of a large number of fluctuators leading to a  $1/f$  noise, but we aim to better understand the effect of a single one on the qubit. The evolution of the electronic states of the qubit as a function of time is calculated by numerical solution of the Schrödinger equation in a multiband framework in which the potential is calculated taking into account the complex environment of the qubit. Such a description is necessary because of the strong sensitivity of the spin-orbit coupling to the potential profile in the vicinity of the hole wave function.

In this paper, we compare the results of numerical calculations with analytical models from the literature that have been established for a two-level system coupled to telegraphic noise, allowing us to understand the evolution of the relaxation time  $T_1$  and dephasing time  $T_2$  as a function of noise intensity and tunneling rate  $\nu$ . However, we show that the potential fluctuations couple with more than two levels and that it is necessary to take a large number of them ( $\sim 20$ ) to simulate the spin evolution as a function of time. This leads us to define another decoherence time  $T_1'$  that represents the mean time the system remains describable as a two-level system. Despite this complexity, we obtain that, for experimentally relevant tunneling rates  $\nu$  below a certain value  $\omega_{th}$ ,  $T_2$  has a remarkable but very simple behavior, being equal to  $2/\nu$  independently of the intensity of the perturbing potential. We also study how the operating conditions (gate bias, magnetic field orientation) affect the dephasing time  $T_2(\omega_{th})$  at the threshold frequency  $\omega_{th}$ . In addition, we obtain that the decoherence time  $T_1'$  is always smaller than the relaxation time  $T_1$  calculated in the two-level model. This reveals that the spin relaxation dynamics is very strongly influenced by the coupling with hole states further away in energy, and thus  $T_1$  cannot be described simply on the basis of the two-level model, a conclusion that should guide future theoretical simulation work.

## II. METHODOLOGY

### A. Calculation of the potential and the hole states in the device

The device presented in Fig. 1 is a metal-oxide-semiconductor field effect transistor (MOSFET) formed by a Si nanowire oriented along [110] (hereinafter, the  $z$  axis). The nanowire has a rectangular section with width (along  $y$ ) of 30 nm [lateral ( $\bar{1}\bar{1}0$ ) facets] and thickness of 10 nm [(001) facets] and is lying on a 25-nm-thick  $\text{SiO}_2$  buried oxide deposited on a doped Si substrate which can be used as a back gate. On top of the channel, there are metal gates with length and separation along  $z$  of 30 nm that partly envelop the channel (over 20 nm). A 4-nm thin layer of  $\text{SiO}_2$  separates the metallic gates from the nanowire. The transistor is covered with  $\text{Si}_3\text{N}_4$ . The central gate (CG) is used to fix the potential that will induce the formation of a quantum dot (with corner

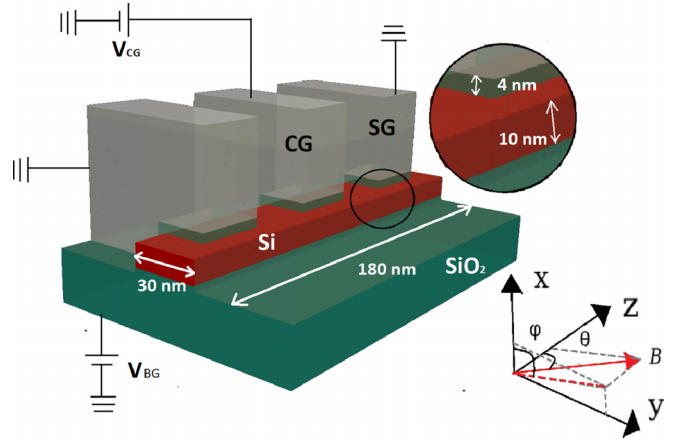


FIG. 1. Schematics of the hole qubit device consisting of a 10-nm-thick Si nanowire channel (red) on top of a buried oxide (green). Top gates (gray) partly cover the nanowire (over 20 nm for a total width of the nanowire of 30 nm). The gate stack is made of  $\text{SiO}_2$  (green). CG represents the central gate that defines the hole quantum dot. SG is the secondary gate discussed in this paper. The orientation of the magnetic field  $\mathbf{B}$  is characterized by the polar angle  $\theta$  and azimuthal angle  $\varphi$  defined in the figure.

states) in the nanowire [40]. Two secondary gates are arranged along the  $z$  axis, to the right and left of the central gate. The central gate is biased at  $V_{CG} = -0.1$  V, and the other gates are grounded in order to confine the hole in the central quantum dot. A static magnetic field  $\mathbf{B}$  is applied along a direction defined by polar ( $\theta$ ) and azimuthal ( $\varphi$ ) angles (see Fig. 1).

The potential induced by the gates or by the presence of a charge impurity in the oxide layer is calculated by solving the Poisson equation linking the charge density  $\rho$  and the dielectric constant  $\epsilon$  that both depend on the position. To solve it, we use the finite difference method which consists in discretizing the equation spatially on a three-dimensional (3D) mesh.

To calculate the electronic structure in our device, we use a six-band  $\mathbf{k} \cdot \mathbf{p}$  model which gives an excellent description of the valence band states, including the effect of spin-orbit coupling. Details on the numerical methods are given in Ref. [40] and are reproduced in Sec. I of the Supplemental Material [46] for convenience. The wave functions of the holes are written as

$$\psi(\mathbf{r}) = \sum_{\alpha} F_{\alpha}(\mathbf{r})u_{\alpha}(\mathbf{r}), \quad (1)$$

where  $F_{\alpha}(\mathbf{r})$  is an envelope function and  $u_{\alpha}(\mathbf{r})$  is a Bloch function in the set  $\{|\frac{3}{2}, +\frac{3}{2}\rangle, |\frac{3}{2}, +\frac{1}{2}\rangle, |\frac{3}{2}, -\frac{1}{2}\rangle, |\frac{3}{2}, -\frac{3}{2}\rangle, |\frac{1}{2}, +\frac{1}{2}\rangle, |\frac{1}{2}, -\frac{1}{2}\rangle\}$ . The envelope functions are solutions of six coupled differential equations obtained from the  $\mathbf{k} \cdot \mathbf{p}$  Hamiltonian  $H_{6kp}$  given in Sec. I of the Supplemental Material [46] in which the wave vector  $\mathbf{k}$  has been substituted by  $-i\nabla$ . These equations are discretized on a finite difference mesh. Even if the quantum dots are effectively decoupled by the action of the lateral gates, periodic boundary conditions are applied along  $z$ . The surface of the wire is considered as a hard wall for the wave function. The effect of the potential vector  $\mathbf{A}$  on the

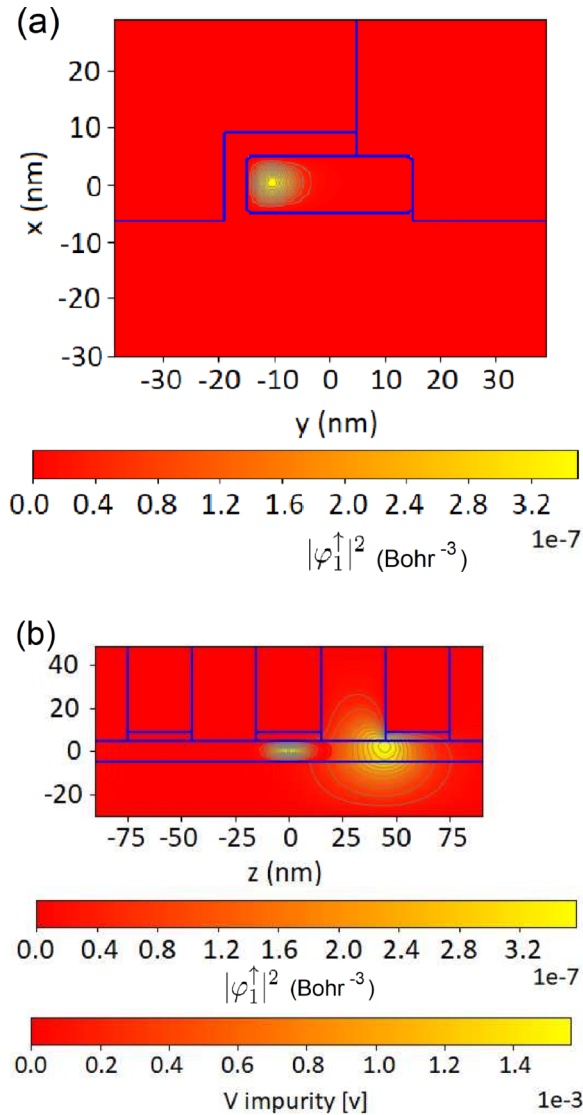


FIG. 2. Isodensity surface of the ground-state hole wave function depicted across (a) transverse ( $xy$  plane at  $z = 0$ ) and (b) longitudinal ( $xz$  plane,  $y = -10$  nm corresponding to the center of the hole wave function) cross sections. The potential induced by a single charge (trap 3) at position  $x = 8.4$  nm,  $y = 0$ , and  $z = 46.0$  nm is also shown in (b).

envelope functions is included through Peierls's substitution [47]. The effect of the magnetic field on the Bloch functions is described by the following Hamiltonian [48]:

$$H_{\text{Bloch}} = -(3\kappa + 1)\mu_B \mathbf{B} \cdot \mathbf{L} + g_0 \mu_B \mathbf{B} \cdot \mathbf{S} = \mu_B \mathbf{B} \cdot \mathbf{K}, \quad (2)$$

where  $\mathbf{L}$  is the (orbital) angular momentum of the Bloch function,  $\mathbf{S}$  is its spin, and  $\kappa = -0.42$  in silicon. The expression of the matrices  $\mathbf{K}$  is given in Sec. I of the Supplemental Material [46].

The hole qubit states are taken as the topmost valence band states. The wave function of the highest hole state is presented in Fig. 2(a) across a transverse section of the MOSFET and in Fig. 2(b) for a longitudinal one.

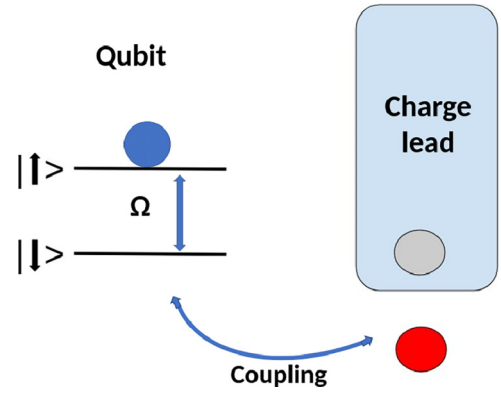


FIG. 3. Model of qubit coupled to a single charge fluctuator. A single electron tunneling between a charge lead, i.e., a gate and a point trap (red circle) induces a sudden change in the electrostatic potential that couples to the qubit hole states. Dephasing and relaxation of the hole spin take place under the effect of this perturbation in the form of a telegraphic noise. Only the two hole levels of lowest energy are depicted for simplicity. The Zeeman energy splitting between them is  $\hbar\Omega$ , in which  $\Omega$  is the Larmor angular frequency.

### B. Fluctuator model and time-dependent Hamiltonian

We consider that the hole qubit is coupled to a charge fluctuator (Fig. 3) which follows a random telegraphic signal  $\chi(t)$  that describes the filling of a localized charge trap in the oxide layer at a distance of 1 nm from a metallic gate, either the central gate (CG) or the secondary gate (SG) shown in Fig. 1. An example of a potential created by a localized charge  $-e$  under the secondary gate is presented in Fig. 2(b). The charge fluctuator is described as a random telegraphic noise [39], i.e.,  $\chi(t)$  takes two values, 0 or 1, with respective probabilities  $p_0$  and  $p_1$ . In the state 0 of  $\chi(t)$ , the trap is empty, and in the state +1, a charge  $-e$  has tunneled from the gate to the trap with a transition rate  $\nu_{0 \rightarrow 1} = \nu[1 - f_{\text{FD}}(\epsilon_0)]$  where  $\nu$  is the tunneling rate,  $f_{\text{FD}}$  is the Fermi-Dirac distribution function, and  $\epsilon_0$  is the position of the trap level with respect to the Fermi level in the reservoir (gate). Here, we assume for simplicity  $\epsilon_0 = 0$ ,  $\nu_{0 \rightarrow 1} = \nu/2$ ,  $\nu_{1 \rightarrow 0} = \nu - \nu_{0 \rightarrow 1} = \nu/2$ , and  $p_0 = p_1 = 1/2$  [49]. In this model, the ‘‘classical’’ frequency of the telegraphic signal, i.e., the average number of switches per time unit, is given by  $\nu_{cl} = \nu/2$ .

The time-dependent Hamiltonian of the system reads as

$$H(t) = H_0 + \chi(t)U, \quad (3)$$

where  $H_0$  is the Hamiltonian representing the system under the static magnetic field  $\mathbf{B}$  but without any electrical perturbation.  $U$  defines the perturbation when a charge is on the trap.

In order to calculate the evolution of the wave function  $|\psi(t)\rangle = \exp(-i/\hbar \int_0^t H(t')dt')|\psi(0)\rangle$  and the characteristic times  $T_1$ ,  $T_1'$ , and  $T_2$  which will be discussed in the next sections, we solve the time-dependent Schrödinger equation numerically. A Chebyshev polynomial expansion is used to describe the time propagation of the wave function [50]. This approach ensures high numerical stability of the propagator.

### 1. Two-level model

A qubit is generally constructed as a two-level system, the two states corresponding here to the lowest-energy hole states, eigenstates of  $H_0$ , denoted as  $|\varphi_1^\uparrow\rangle$  and  $|\varphi_1^\downarrow\rangle$  in reference to spin-1/2 systems. The Zeeman splitting ( $\propto B$ ) between the two levels [for  $\chi(t) = 0$ ] is written as  $\hbar\Omega$  where  $\Omega$  is the Larmor angular frequency. Rabi oscillations between the two states can be electrically driven by a radio-frequency signal with an angular frequency close to  $\Omega$  on the central front gate [37,40].

The matrices of the Hamiltonian and the perturbation in this basis set are given by

$$H_0 = \frac{\hbar}{2} \begin{pmatrix} \Omega & 0 \\ 0 & -\Omega \end{pmatrix}, \quad U = \begin{pmatrix} u_{\uparrow\uparrow} & u_{\uparrow\downarrow} \\ u_{\downarrow\uparrow}^* & u_{\downarrow\downarrow} \end{pmatrix}. \quad (4)$$

The electrostatic potential induced by the trapped charge does not explicitly involve spin, but the matrix elements of  $U$  depend on  $B$  through  $|\varphi_1^\uparrow\rangle$  and  $|\varphi_1^\downarrow\rangle$ . The coupling terms between these opposite-spin states result from spin-orbit coupling and time-reversal symmetry breaking under the effect of the magnetic field  $\mathbf{B}$ . As shown in Sec. II of the Supplemental Material [46], the matrix elements of  $U$  behave as

$$\begin{aligned} u_{\uparrow\downarrow} &= \eta_{\uparrow\downarrow}(\mathbf{b})B, \\ u_{\uparrow\uparrow} &= u_0 + \eta_{\uparrow\uparrow}(\mathbf{b})B, \\ u_{\downarrow\downarrow} &= u_0 + \eta_{\downarrow\downarrow}(\mathbf{b})B, \end{aligned} \quad (5)$$

in which  $\mathbf{b} = \mathbf{B}/B$  and therefore  $\eta_{\uparrow\downarrow}$ ,  $\eta_{\uparrow\uparrow}$ , and  $\eta_{\downarrow\downarrow}$  just depend on the orientation of  $\mathbf{B}$ .  $u_0$  is a rigid shift of the two energy levels under the effect of the perturbation.

The interaction of the qubit with its environment (Fig. 3) causes a loss of information, called decoherence. It is usually separated in two processes, relaxation of characteristic time  $T_1$  and dephasing of characteristic time  $T_2$  [39,51]. We obtain  $T_1$  and  $T_2$  by calculating the evolution with time of  $\langle\langle\sigma_i(t)\rangle\rangle = \langle\psi(t)|\sigma_i|\psi(t)\rangle_{\{E\}}$  with  $i = 1, 2, 3$ .  $\sigma_1$ ,  $\sigma_2$ , and  $\sigma_3$  are the  $2 \times 2$  Pauli matrices written in the basis of  $|\varphi_1^\uparrow\rangle$  and  $|\varphi_1^\downarrow\rangle$  (they are not written  $\sigma_x$ ,  $\sigma_y$ , and  $\sigma_z$  since  $x$ ,  $y$ , and  $z$  refer to the geometrical axes of the system). The subscript  $\{E\}$  means that an average is taken over many (1000) realizations of the telegraphic noise, i.e., of the environment.

The relaxation is the loss of information by the process  $|\varphi_1^\uparrow\rangle \leftrightarrow |\varphi_1^\downarrow\rangle$  due to the stochastic variations of the nondiagonal term  $\chi(t)u_{\uparrow\downarrow}$  of the Hamiltonian. Starting with the condition  $|\psi(0)\rangle = |\varphi_1^\uparrow\rangle$ , we calculate  $T_1$  by fitting with an exponential function the decay of  $\sigma_{\parallel}(t) = \langle\langle\sigma_3(t)\rangle\rangle$  over time.

The dephasing comes from the changes  $\delta\phi(t)$  of the phase characterizing the spin precession due to the stochastic variations of the terms of the Hamiltonian,  $\chi(t)U$ . Indeed, in the  $\chi(t) = 1$  state, the Larmor angular frequency changes to  $\Omega'$ , where  $\hbar\Omega'$  is the Zeeman splitting obtained by diagonalization of  $H_0 + U$ . As discussed in Sec. III of the Supplemental Material [46], it will be interesting to define the (threshold) angular frequency

$$\omega_{th} = |\Omega - \Omega'| \quad (6)$$

that characterizes the change of phase velocity (usually  $\omega_{th} \ll \Omega$ ).  $\hbar\omega_{th}$  represents the change in the Zeeman splitting between the two states of the fluctuator. We deduce from Eq. (5)

that  $\omega_{th} \propto B$  in most cases (see Sec. III B of the Supplemental Material [46]).

A measure of the phase coherence is given by the quantity  $\langle\exp(i\delta\phi(t))\rangle_{\{E\}}$  [39]. Equivalently, we have calculated the quantity  $m(t) = |\langle\langle\sigma_1(t)\rangle\rangle + i\langle\langle\sigma_2(t)\rangle\rangle|$  using the initial condition  $|\psi(0)\rangle = (|\varphi_1^\uparrow\rangle + |\varphi_1^\downarrow\rangle)/\sqrt{2}$ . The decay of  $m(t)$  from 1 to 0 comes from the dephasing between the different realizations of the potential fluctuations.  $T_2$  is obtained by fitting with an exponential function the decay of  $m(t)$  over time. It is important to note that for  $\nu < \omega_{th}$ ,  $m(t)$  exhibits damped oscillations at a frequency of the order of  $\omega_{th}$  [39] (see Sec. VIII of the Supplemental Material [46]). In this case,  $T_2$  is obtained from the exponential decay of the envelope.

### 2. Multilevel model

The perturbation generated by the fluctuator induces coupling terms that are not limited to the two states considered above. We have therefore considered a model integrating  $2N$  hole states. With the matrices of  $H_0$  and  $U$  written in this basis, we compute the propagation of the hole wave function as a function of time starting from the same initial conditions. We deduce the observable  $m(t)$  from which we obtain the characteristic time  $T_2$ , assuming that  $\sigma$  acts only in the subspace formed by  $|\varphi_1^\uparrow\rangle$  and  $|\varphi_1^\downarrow\rangle$ . As a matter of fact, during the evolution as a function of time, the weight of the wave function of the hole on the two initial states,  $p_1(t) = |\langle\varphi_1^\uparrow|\psi(t)\rangle|^2 + |\langle\varphi_1^\downarrow|\psi(t)\rangle|^2$ , decreases under the effect of the couplings to the other states. From the exponential decay of  $\langle p_1(t) \rangle_{\{E\}}$ , averaged over all the realizations of the telegraphic noise, we deduce another decoherence time, which we call  $T_1'$ , following the methodology described in Appendix A.

It is important to note that the elements composing the perturbation  $U$  are not independent since they are matrix elements of the same electrostatic potential. The same effect is at the origin of all the decoherence mechanisms considered here.

### 3. Time interval, frequency range, and trap position

We consider (except where otherwise stated) a magnetic field of 0.2712 T oriented along the direction characterized by  $\theta = 90^\circ$  and  $\varphi = 45^\circ$  (Fig. 1) which leads to a Larmor frequency  $\Omega/(2\pi)$  of 10 GHz. This forces us to use a time step of  $10^{-12}$  s for the numerical solution of the time-dependent Schrödinger equation for  $\nu \leq 2 \times 10^{11} \text{ s}^{-1}$ ,  $10^{-13}$  s for  $\nu = 2 \times 10^{12} \text{ s}^{-1}$ ,  $10^{-14}$  s for  $\nu = 2 \times 10^{13} \text{ s}^{-1}$ , and  $10^{-15}$  s for  $\nu = 2 \times 10^{14} \text{ s}^{-1}$ . The maximum simulation time has been limited to  $10^{-4}$  s. We thus considered  $\nu$  between  $2 \times 10^6$  and  $2 \times 10^{14} \text{ s}^{-1}$ . However, the laws of variation of the characteristic times as a function of  $\nu$  will allow us to extrapolate them to smaller tunneling rates  $\nu$  which often characterize telegraphic noises [39].

We have considered three positions for the trap (Table I). Traps 1 and 2 are under the central gate, and trap 3 is under the secondary gate. Trap 1 is the closest to the hole quantum dot. It therefore induces the strongest perturbation potential on the hole. In contrast, trap 3 induces the lowest perturbation.

TABLE I. Charge traps considered in this paper. Position: The coordinates  $x$ ,  $y$ , and  $z$  are defined with respect to the axes specified in Figs. 1 and 2. Characteristics deduced from the perturbation matrix: angular frequency  $\omega_{th}$  [Eq. (7)] and modulus  $|u_{\uparrow\downarrow}|$  of the nondiagonal matrix element.

Trap	Coordinates (nm)			Gate	$\omega_{th}$ (s <sup>-1</sup> )	$ u_{\uparrow\downarrow} $ ( $\mu$ eV)
	$x$	$y$	$z$			
Trap 1	8.4	0.0	0.0	Central	$1.063 \times 10^9$	1.4594
Trap 2	8.4	4.0	14.0	Central	$5.469 \times 10^8$	0.4381
Trap 3	8.4	0.0	46.0	Secondary	$3.039 \times 10^7$	0.0248

### III. RESULTS AND DISCUSSION

#### A. Quantum dot energy levels and hole state dynamics

The ten highest electronic energy levels calculated for the qubit are shown in Fig. 4(a). The level defining the fundamental hole state, the highest in electron energy, is twice degenerate in the absence of a magnetic field. This level is relatively detached from the others, and the Zeeman splitting is not visible at the scale of the figure. Therefore the electrostatically induced confinement by the central gate defines a two-state system.

Nevertheless, Fig. 5(a) shows the evolution of  $p_1(t)$ , the average total weight of the hole wave function on the  $\varphi_1^\sigma$  qubit states as a function of time, for a charge fluctuating

between the central gate and trap 1 at average frequency  $\nu = 2 \times 10^9$  s<sup>-1</sup>.  $p_1(t)$  decreases as a function of time, from which we can deduce  $T_1'$  as described in Appendix A. This results from the coupling of the state  $\varphi_1^\uparrow$  with the other states  $\varphi_n^{\uparrow\downarrow}$  of the system, due to the presence of a charge on trap 1. Interestingly, this coupling is much larger with some states outside the doublet ( $n > 1$ ) than with  $\varphi_1^\downarrow$ . This is demonstrated in Fig. 4(b), which shows the coupling strength defined as the ratio between a matrix element of  $U$  and the energy splitting between the corresponding two states. This coupling strength is important between states of the same doublet (because the denominator is small), but it remains of the same order of magnitude with a large number of multiplets much further away in energy.

Figures 5(b) and 5(c) show the decay of  $\sigma_{\parallel}(t)$  and  $m(t)$  obtained under the same noise conditions. We deduce the characteristic times  $T_1$  and  $T_2$  by fitting with an exponential.

Figure 4(d) shows that diagonal terms of the perturbation  $u_n^{\uparrow\uparrow} = \langle \varphi_n^\uparrow | U | \varphi_n^\uparrow \rangle$  or  $u_n^{\downarrow\downarrow} = \langle \varphi_n^\downarrow | U | \varphi_n^\downarrow \rangle$  are relatively independent of the spin orientation in each doublet  $n$ , their main effect being a global shift in energy of the electronic levels. The difference  $\delta_n = u_n^{\uparrow\uparrow} - u_n^{\downarrow\downarrow}$ , which for  $n = 1$  will determine the main dephasing effect (see below), is small and is strongly dependent on  $n$  [Fig. 4(c)]. It is shown in Sec. II of the Supplemental Material [46] that  $\delta_n$  is zero for  $B = 0$  and is given in perturbation theory by a sum of terms scaling as  $|E_n - E_m|^{-1}$  with  $m \neq n$ . This explains why  $\delta_1 = u_1^{\uparrow\uparrow} - u_1^{\downarrow\downarrow} = u_{\uparrow\uparrow} - u_{\downarrow\downarrow}$

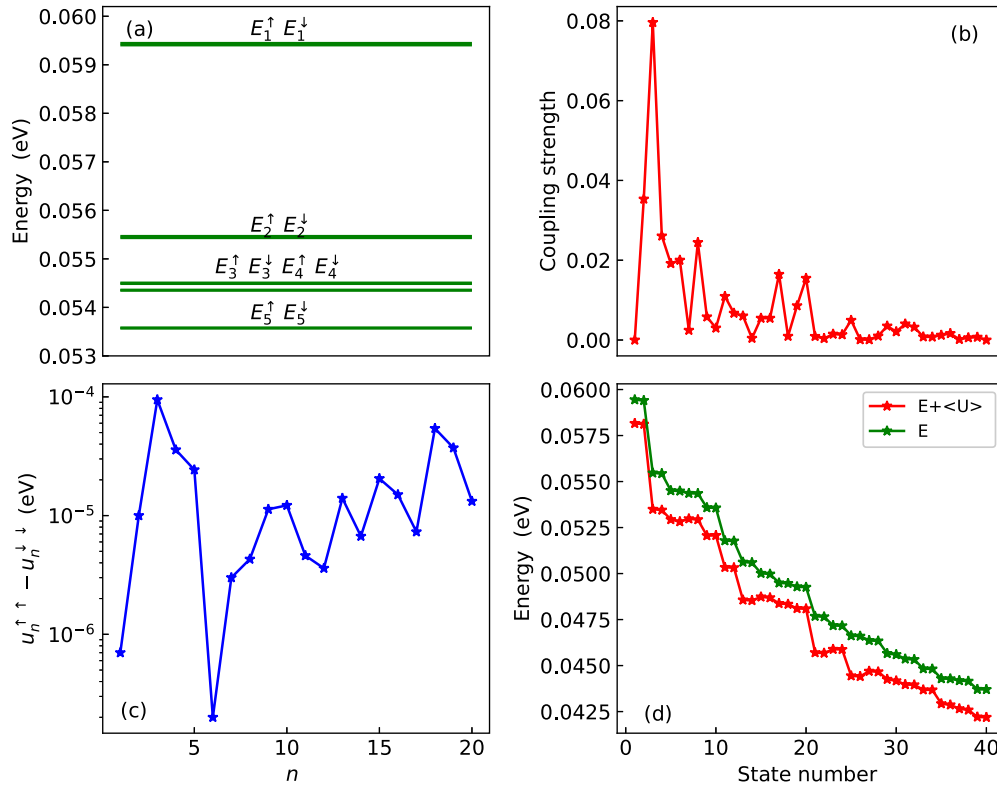


FIG. 4. (a) Highest electronic energy levels calculated for the hole qubit. (b) Coupling strength defined as the ratio  $|\langle \varphi_1^\uparrow | U | \varphi_n^{\uparrow\downarrow} \rangle| / |E_1^\uparrow - E_n^{\uparrow\downarrow}|$ . (c)  $\delta_n = \langle \varphi_n^\uparrow | U | \varphi_n^\uparrow \rangle - \langle \varphi_n^\downarrow | U | \varphi_n^\downarrow \rangle = u_n^{\uparrow\uparrow} - u_n^{\downarrow\downarrow}$  vs  $n$ . (d) Unperturbed level energies  $E_n^{\uparrow\downarrow}$  (green) and perturbed level energies  $E_n^{\uparrow\downarrow} + \langle \varphi_n^{\uparrow\downarrow} | U | \varphi_n^{\uparrow\downarrow} \rangle$  (red) presented according to the state number defined as  $2n - 1$  for  $|\varphi_n^\uparrow\rangle$  states and  $2n$  for  $|\varphi_n^\downarrow\rangle$  states. In (b)–(d), all results are for trap 1. (b) and (d) share the same horizontal axis.

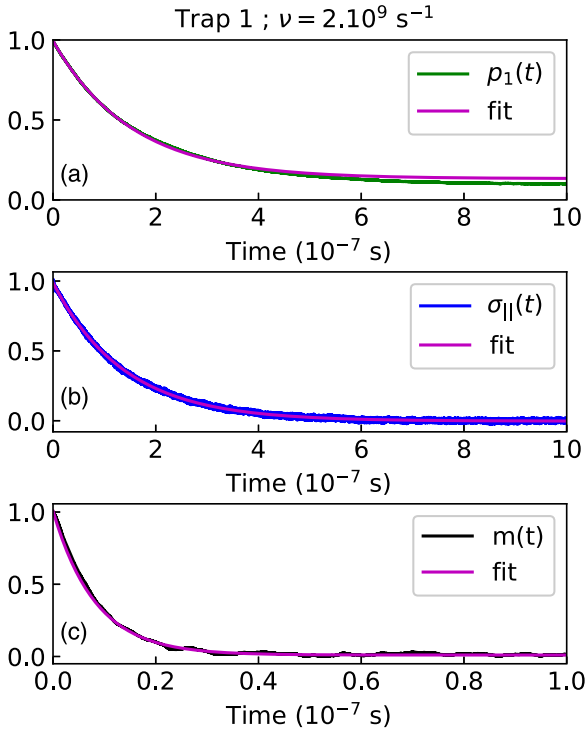


FIG. 5. Evolution of  $p_1(t)$  (a),  $\sigma_{\parallel}(t)$  (b), and  $m(t)$  (c) for trap 1 and  $\nu = 2 \times 10^9 \text{ s}^{-1}$ , calculated in the multilevel model ( $N = 20$ ). The curves in pink are fits by an exponential law. For  $p_1(t)$ , the fit is made in the range  $0.5 \leq p_1 \leq 1$  only.

is small because the fundamental level ( $n = 1$ ) is strongly detached from the others in energy.

## B. Characteristic times for the two-level system

Even if our numerical simulations show the non-negligible role of high-energy hole states, it is useful to consider the two-level system ( $N = 1$ ). Relaxation ( $T_1$ ) and dephasing ( $T_2$ ) times calculated for trap 1 (Table I) in the two-level model are therefore presented in Fig. 6.

### 1. Analytical model: Dephasing time

It is interesting to relate the variations of  $T_2(\nu)$  to those of  $T_2^*(\nu)$ , the dephasing time obtained in the so-called pure dephasing model, i.e., when the matrix  $U$  [Eq. (4)] is purely diagonal, or more generally when  $|u_{\uparrow\uparrow} - u_{\downarrow\downarrow}| \gg |u_{\uparrow\downarrow}|$ . In this case, the (threshold) angular frequency can be written as (Sec. III of the Supplemental Material [46])

$$\omega_{th} \approx |u_{\uparrow\uparrow} - u_{\downarrow\downarrow}|/\hbar, \quad (7)$$

in which  $|u_{\uparrow\uparrow} - u_{\downarrow\downarrow}|$  [ $\delta_1$  in Fig. 4(c)] represents the variation of the energy splitting between the two states when the fluctuator switches. In the high-frequency limit ( $\nu \gg \omega_{th}$ ), the phase undergoes many random changes  $\delta\phi(t)$  over a time interval of the order of  $2\pi/\omega_{th}$ , so that  $\delta\phi(t)$  can be viewed as a continuous random variable characterized by a Gaussian probability distribution. In this Gaussian limit, the dephasing time is given by  $T_2^* = 4\nu/\omega_{th}^2$  [45,49,52]. The linear dependence on the frequency  $\nu$  reflects the fact that the two-level system becomes more and more insensitive to the random

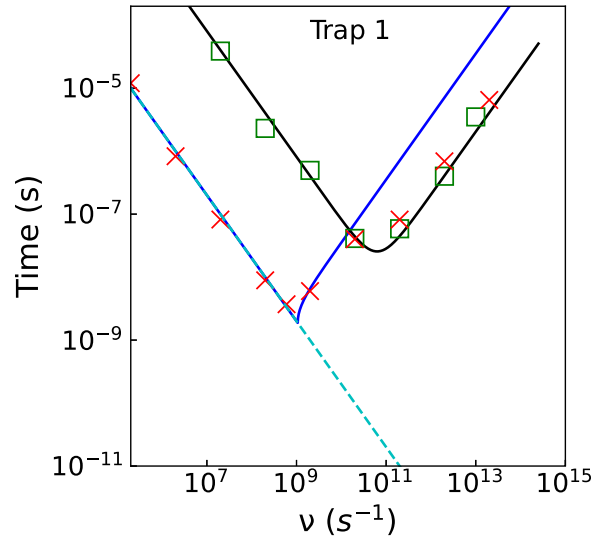


FIG. 6. Characteristic lifetimes  $T_1$  (green squares) and  $T_2$  (red crosses) vs tunneling rate  $\nu$  calculated in the two-level model for trap 1. Solid lines depict the analytical expressions for  $T_1$  (black) and  $T_2^*$  (blue), as given by Eqs. (10) and (8), respectively, using  $\omega_{th}$  and  $|u_{\uparrow\downarrow}|$  of Table I. The dashed turquoise line shows a time varying as  $2/\nu$ . At  $\nu \gg \Omega$ ,  $T_2 \approx 2T_1$ .

perturbation as this one varies more and more rapidly. In this case, the splitting between the two levels is self-averaged to a certain value, the width being  $\propto 1/T_2^*$  [45].

In the opposite limit of low frequencies ( $\nu \ll \omega_{th}$ ), the Gaussian approximation is no longer valid, and the dephasing time is then given by  $T_2^* = 2/\nu = 1/\nu_{cl}$  [45,49,52] (see also Sec. III of the Supplemental Material [46]). In this regime, the coherence is simply determined by the probability  $\exp(-t/T_2^*)$  that the qubit has not suffered any switch of the fluctuator over a time  $t$ . In other words, the coherence is lost from the moment when the fluctuator has changed state.

Extending the analysis to all frequencies, an expression for  $T_2^*$  was derived in the pure dephasing regime [49,52]:

$$T_2^* = \begin{cases} \frac{2}{\nu - \sqrt{\nu^2 - \omega_{th}^2}} & \text{for } \nu \geq \omega_{th} \\ 2/\nu & \text{for } \nu < \omega_{th}, \end{cases} \quad (8)$$

which shows that the angular frequency  $\omega_{th} = |\Omega - \Omega'|$  is therefore a threshold between two distinct regimes.

In the general case, beyond the pure dephasing model, the dephasing time becomes [39]

$$T_2 = \left( \frac{1}{T_2^*} + \frac{1}{2T_1} \right)^{-1}. \quad (9)$$

### 2. Analytical model: Relaxation time

The spin relaxation is induced by the nondiagonal terms of the  $U$  matrix. Using various approaches such as the Bloch-Redfield theory [39], the relaxation rate is determined by the noise spectrum at frequency  $\Omega$ . In the case of telegraphic noise, this gives the following expression for  $T_1$ :

$$T_1 = \frac{\hbar^2}{|u_{\uparrow\downarrow}|^2} \frac{\nu^2 + \Omega^2}{\nu}, \quad (10)$$

which reflects a resonance effect. Relaxation is most effective when the fluctuator frequency coincides with the Larmor angular frequency. At low tunneling rate  $\nu \ll \omega_{th} \ll \Omega$ ,  $T_1$  also varies as  $1/\nu$ , like  $T_2^*$  but with a prefactor  $(\hbar\Omega/|u_{\uparrow\downarrow}|)^2$  instead of 2 (another derivation of this expression is presented in Sec. V of the Supplemental Material [46]). Table I shows that  $|u_{\uparrow\downarrow}| \ll \hbar\Omega$  for the traps considered here; therefore  $T_1 \gg T_2^*$  and  $T_2 \approx T_2^*$  from Eq. (9).

### 3. Discussion of numerical results in comparison with analytical laws

Figure 6 shows that the calculated values of  $T_1$  follow Eq. (10), which translates the resonance effect between the quantum oscillator formed by the two-level system and the classical fluctuator.

The dephasing time  $T_2$  deduced from the time simulations is also in excellent agreement with the analytical expression for  $T_2^*$  given by Eq. (8), except at high frequency where  $T_1$  becomes smaller than  $T_2^*$  and therefore  $T_2 \approx 2T_1$  [Eq. (9)].

### C. Characteristic times for the multilevel system

The calculated characteristic times  $T_2$  and  $T_1'$  for the three traps in the multilevel model are shown in Fig. 7.

#### 1. Relaxation time for trap 1

The relaxation time  $T_1'$  is much smaller than  $T_1$  obtained in the two-level model, in particular at high frequency ( $>10^{10} \text{ s}^{-1}$ ) where  $T_1'$  continues to decrease with  $\nu$  to reach a minimum for  $\nu$  near  $10^{13} \text{ s}^{-1}$ . This is due to the coupling with higher-energy hole levels, outside the doublet. For frequencies below  $\approx 10^{12} \text{ s}^{-1}$ ,  $T_1'$  varies approximately as  $1/\nu$ , as given by Eq. (10) for  $T_1$  for  $\nu \ll \Omega$  but with a smaller prefactor.

The fact that  $T_1'$  is found to be much smaller than  $T_1$  given by Eq. (10) means that the two-level model is not valid for the description of the spin relaxation, the latter being strongly influenced by the coupling to higher-energy hole levels.

#### 2. Dephasing time for trap 1

Remarkably, the values of  $T_2$  coincide with those obtained in the two-level model for  $\nu$  less than or just above  $\omega_{th}$  given in Table I. In this case, the two-level model is perfectly justified. For higher tunneling rates, the values of  $T_2$  approximately follow those of  $T_1'$ . This behavior indicates that the dephasing is impacted by the other decoherence phenomena, which is expected because they are fundamentally intertwined since they all result from the same electrical disturbance, i.e., diagonal and nondiagonal terms are present at the same time in the matrix of  $U$ .

#### 3. Results for traps 2 and 3

Figure 7(b) shows the same behavior for trap 2 located at a larger distance from the center of the qubit state. Consequently, the characteristic times  $T_1$  (for the two-level model) and  $T_1'$  have higher values than for trap 1, since the perturbation induced by the fluctuator is less strong. For the same reason,  $\omega_{th}$  shifts to a lower frequency. This behavior is even more visible in the case of trap 3 located under the secondary

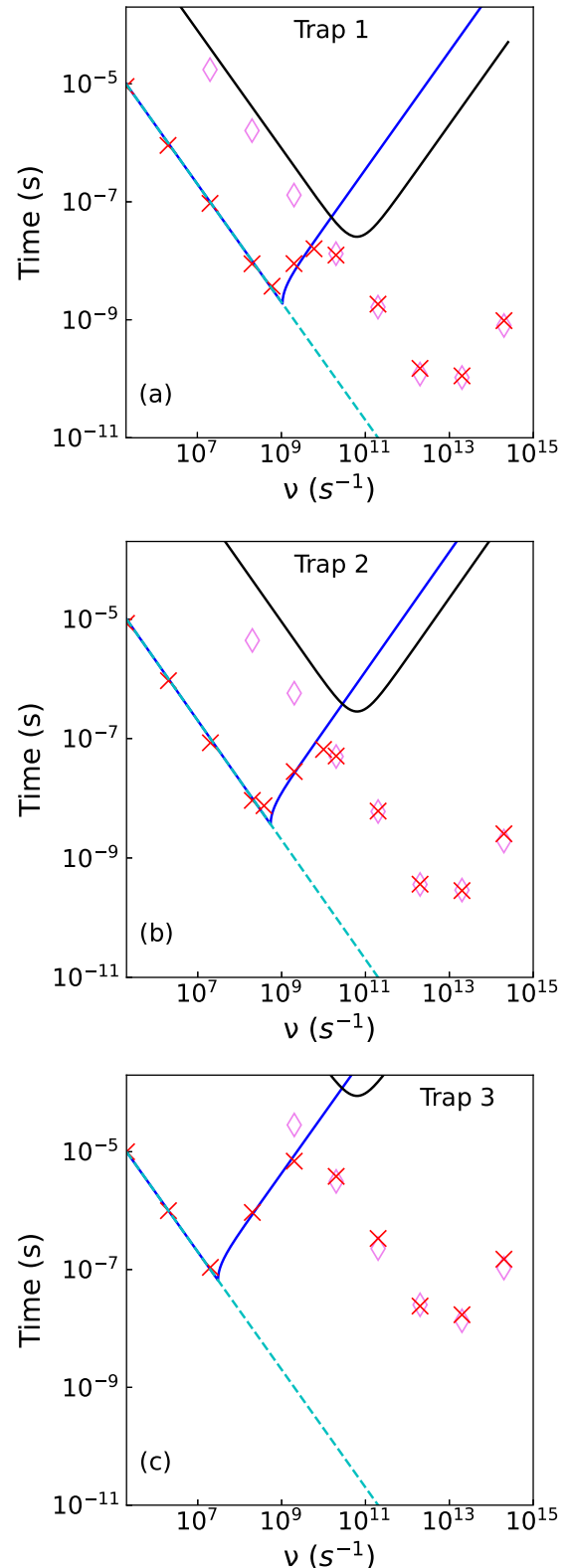


FIG. 7. (a) Characteristic lifetimes  $T_1'$  (magenta diamonds) and  $T_2$  (red crosses) vs tunneling rate  $\nu$  calculated in the multilevel model ( $N = 10$ ) for trap 1. Solid lines depict the analytical expressions for  $T_1$  (black) and  $T_2^*$  (blue) of the two-level model, as given by Eqs. (10) and (8), respectively, using  $\omega_{th}$  and  $|u_{\uparrow\downarrow}|$  of Table I. (b) Same for trap 2. (c) Same for trap 3. In (a)–(c) the dashed turquoise line shows a time varying as  $2/\nu$ .

gate [Fig. 7(c)].  $\omega_{th}$  is pushed to even lower frequencies (Table I). The comparison between Figs. 7(a)–7(c) shows that the two-level model for  $T_1$  becomes even less valid when the trap moves away from the qubit, when  $T_1$  becomes very long. Indeed, as the distance between the trap and the qubit increases, the coupling terms all decrease, but those with the higher-energy states decrease less rapidly than those within the doublet of states (Sec. VI of the Supplemental Material [46]). This can be explained by the larger spatial extension of higher-energy hole states.

A remarkable result of Fig. 7 is that, for  $\nu < \omega_{th}$ ,  $T_2 \approx T_2^*$  is given by  $2/\nu = 1/\nu_{cl}$ ; whatever the position of the trap, only the value of  $\omega_{th}$  changes between the different cases. This is the likely regime for a qubit in cryogenic conditions for which the tunneling rates are normally low [39,45,53]. This means that the coherence of the qubit is entirely and solely determined by the average time between two changes of state of the fluctuator. The qubit remains coherent as long as the fluctuator has not changed its state.

#### IV. INFLUENCE OF THE BACK-GATE BIAS AND THE MAGNETIC FIELD ORIENTATION

In a recent theoretical work including numerical simulations on the same hole qubit as the one studied here [40], the manipulation of the hole spin by a radio-frequency electrical excitation applied on the central gate has been modeled. It has been shown that the Rabi frequency depends in a complex way on the orientation of the magnetic field and the back-gate potential  $V_{BG}$ . The latter allows one to control the shape and the symmetry of the wave function of the hole, on which depends the effective spin-orbit coupling felt and consequently the  $g$  tensor defining the response of its spin to the magnetic field.

In fact, all these quantities depend essentially on the component of the internal electric field along  $y$ , which is controlled by the imbalance between front- and back-gate voltages [40]. This component is nonzero because of the asymmetry of the structure (Fig. 1). The component of the field along  $x$ , although dominant in intensity, plays a much more minor role due to the strong vertical confinement of the hole states. The  $y$  component of the field influences the wave function of the ground state of the hole: not only its position along  $y$  but also the respective weight of heavy and light hole components, which determines the effective spin-orbit coupling applying to the hole (Sec. IV of the Supplemental Material [46]).

Interestingly, it was found in Ref. [40] that, for  $V_{BG} = -0.15$  V, the qubit is placed in a configuration where the spin is largely insensitive to radio-frequency excitation on the central gate, the Rabi frequency showing a sharp minimum. In this case, the wave function of the hole is centered in the cross section of the nanowire and presents an approximate inversion symmetry which tends to reduce the action of the spin-orbit coupling on the hole. At this voltage, the influence of the Johnson-Nyquist noise is minimized, as well as the coupling to phonons but to a lesser extent [37].

In this context, we consider the effect of  $V_{BG}$  and the magnetic field orientation on the dephasing time  $T_2$ . As discussed earlier, the evolution of  $T_2$  as a function of  $\nu$  is defined by an angular frequency  $\omega_{th}$  which delineates the low- and high-

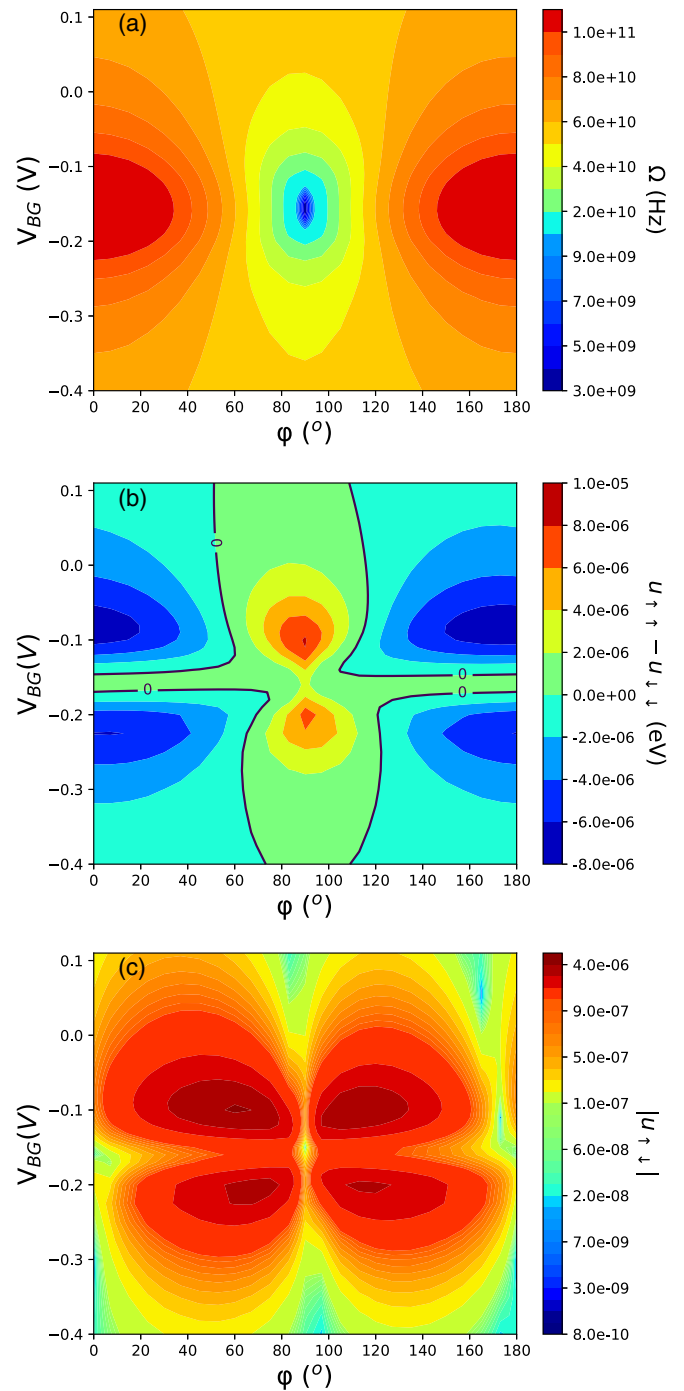


FIG. 8. Two-dimensional plots of (a) the Larmor frequency  $\Omega$ , (b)  $u_{\uparrow} - u_{\downarrow}$ , and (c)  $|u_{\uparrow} - u_{\downarrow}|$  for trap 1 vs back-gate bias  $V_{BG}$  and angle  $\phi$  of  $B$  in the  $xy$  plane ( $\theta = 90^\circ$ ). The 2D plots are made on a discrete grid of  $25 \times 40$  points. (b) The contours corresponding to  $u_{\uparrow} - u_{\downarrow} = 0$  are indicated by black lines.

frequency regimes of the spin response to the fluctuator. It is therefore interesting to look for situations where  $u_{\uparrow} - u_{\downarrow} = 0$  and therefore  $T_2(\omega_{th}) = 2/\omega_{th} = 2\hbar/|u_{\uparrow} - u_{\downarrow}|$  should diverge.

Figure 8 presents the variations of  $\Omega$  and  $u_{\uparrow} - u_{\downarrow}$  as a function of  $V_{BG}$  and  $\phi$ , for  $\theta = 90^\circ$ , i.e., for a magnetic field



in the plane perpendicular to the axis of the nanowire, the field strength remaining fixed at its initial value. Figure 8(b) shows that the 2D map  $u_{\uparrow\uparrow} - u_{\downarrow\downarrow} = f(V_{\text{BG}}, \varphi)$  is divided into regions of positive or negative values, which means that  $u_{\uparrow\uparrow} - u_{\downarrow\downarrow} = 0$  at the boundaries. Consequently, this result suggests the existence of “sweet” lines [30,44] along which  $T_2(\omega_{th})$  should become very long (but not infinite for reasons discussed in Sec. V A).

Zeros of  $u_{\uparrow\uparrow} - u_{\downarrow\downarrow}$  are present, in particular, along a horizontal line  $V_{\text{BG}} \approx -0.15$  V, in the same configuration where the spin becomes relatively insensitive to electrical noise on the central gate [40]. Remarkably, there are also two (almost) straight vertical lines for which  $u_{\uparrow\uparrow} - u_{\downarrow\downarrow} \approx 0$ , at  $\varphi \approx 55^\circ$  and  $\varphi \approx 125^\circ$ . These can be explained as follows.

As demonstrated in Ref. [40] and in Sec. IV of the Supplemental Material [46], the effective Zeeman Hamiltonian of the system can be written in the  $g$ -matrix formalism. For  $\mathbf{B}$  in the  $xy$  plane, the Zeeman splitting is

$$\hbar\Omega = \mu_B B \sqrt{g_x^2 \cos^2 \varphi + g_y^2 \sin^2 \varphi}. \quad (11)$$

It is shown in Ref. [44] that the respective weight of the hole wave function on the heavy and light hole states determines the relative magnitude of the factors  $g_x$  and  $g_y$ . It follows that

$$\frac{\partial g_x}{\partial V} \approx -\frac{\partial g_y}{\partial V}, \quad (12)$$

where  $V$  can be any potential whose main effect on the  $g$  factors comes from the variation of the electric field along  $y$ . Our calculations show that this is the case for  $V_{\text{BG}}$  or for the potential induced by the fluctuating charge.

Under these conditions, it is interesting to consider situations where the Zeeman splitting [Eq. (11)] becomes relatively independent of the potential  $V_{\text{BG}}$ . Using Eq. (12) with  $V = V_{\text{BG}}$ , we deduce in Sec. IV of the Supplemental Material [46] that  $(\partial \hbar\Omega)/(\partial V_{\text{BG}}) = 0$  for

$$\varphi \approx \frac{\pi}{2} \pm \arctan \sqrt{\frac{g_x}{g_y}}. \quad (13)$$

Therefore the compensation between  $\partial g_x/\partial V$  and  $\partial g_y/\partial V$  [Eq. (12)] leading to Eq. (13) explains the straight vertical contour lines in the 2D plot of the Larmor frequency at  $\varphi \approx 90 \pm 34^\circ$  for  $g_x/g_y \approx 2/3$  [Fig. 8(a)]. The existence of these sweet lines has been revealed experimentally in Ref. [44], where a strong enhancement of the coherence times was measured when the Larmor frequency  $\hbar\Omega$  is least dependent on the gate voltages.

The  $g$ -matrix model also allows us to derive analytical expressions for the diagonal matrix elements  $u_{\uparrow\uparrow}$  and  $u_{\downarrow\downarrow}$  of  $\delta H$  describing the perturbation brought by the fluctuating charge (Sec. IV of the Supplemental Material [46]). Remarkably, we find in this simplified model that  $u_{\uparrow\uparrow} - u_{\downarrow\downarrow}$  cancels out when Eqs. (12) and (13) are verified exactly,  $V$  representing the potential induced by the charge.

Additional 2D plots of  $\Omega$  and  $u_{\uparrow\uparrow} - u_{\downarrow\downarrow}$  are presented in Sec. VII of the Supplemental Material [46], versus  $\theta$  and  $\varphi$ , for the three traps. Sweet lines are clearly visible on these figures for  $\varphi$  approximately given by Eq. (13). We conclude

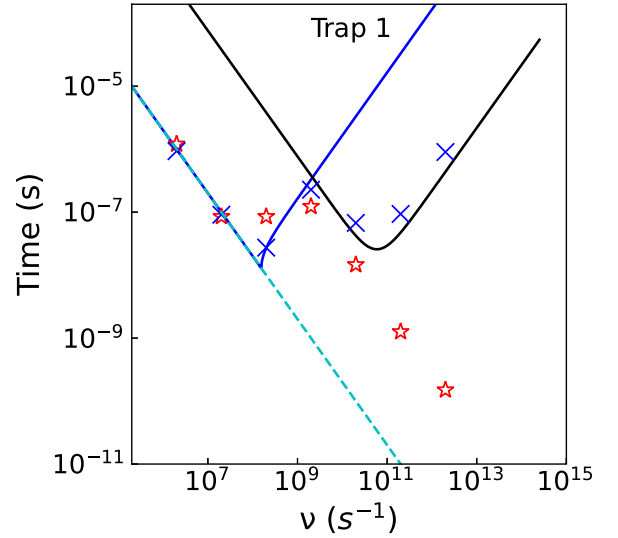


FIG. 9. Characteristic lifetimes  $T_2$  vs tunneling rate  $\nu$  calculated in the two-level model (blue crosses) and multilevel ( $N = 10$ ) model (red stars) for trap 1, for  $V_{\text{BG}} = 0$  V,  $\varphi = 52.6^\circ$ ,  $\theta = 90^\circ$ , and  $\hbar\Omega = 3.88 \times 10^{-5}$  eV, in a situation where  $u_{\uparrow\uparrow} - u_{\downarrow\downarrow} \approx 0$  eV and  $|u_{\uparrow\downarrow}| = 1.41 \times 10^{-6}$  eV. The black solid line depicts the analytical expression for  $T_1$  of the two-level model, as given by Eq. (10). The dashed turquoise line shows a time varying as  $2/\nu$ .

that their existence is relatively robust to the position of the trap [44].

## V. DISCUSSION OF THE RESULTS

### A. Discussion of $T_2$

The existence of “sweet” spots where the dephasing of the spin precession is strongly reduced is now much discussed in the literature [30,40–44,54,55]. The results presented in the previous section could suggest the existence of sweet lines [in the  $(V_{\text{BG}}, \varphi)$  or  $(\theta, \varphi)$  operating spaces] for the noise induced by a single charge fluctuator, but this conclusion should be immediately relativized, for two reasons.

First, for a “slow” fluctuator ( $\nu$  smaller than  $\omega_{th}$ ),  $T_2(\nu)$  is given by  $2/\nu$ , independently of the field or potential conditions. Second, even if we place the system in a situation where  $u_{\uparrow\uparrow} - u_{\downarrow\downarrow} = 0$ , this does not mean that  $\omega_{th} \rightarrow 0$  and  $T_2 \rightarrow \infty$  because the nondiagonal term  $u_{\uparrow\downarrow}$  is not zero (and is even usually maximal [30]). This is clearly visible by comparing, in Figs. 8(b) and 8(c),  $u_{\uparrow\downarrow} \neq 0$  along the lines where  $u_{\uparrow\uparrow} - u_{\downarrow\downarrow} = 0$ . We show in Sec. III of the Supplemental Material [46] that the angular frequency  $\omega_{th} = |\Omega - \Omega'|$  is given in the case  $|u_{\uparrow\uparrow} - u_{\downarrow\downarrow}| \ll |u_{\uparrow\downarrow}|$  by

$$\omega_{th} \approx \frac{2|u_{\uparrow\downarrow}|^2}{\hbar^2 \Omega}. \quad (14)$$

It is interesting to note that  $\omega_{th}$  [and therefore  $T_2(\omega_{th}) = 2/\omega_{th}$ ] given in Eq. (14) is not of the same order in  $U$  as in Eq. (7). The physics discussed here only reveals itself when  $u_{\uparrow\uparrow} - u_{\downarrow\downarrow} \approx 0$ .

Figure 9 shows the evolution of  $T_2$  as a function of  $\nu$  when the system is placed at a specific point on a sweet

line of Fig. 8(b). In the chosen case, Eq. (14) gives  $\omega_{th} = 1.6 \times 10^8 \text{ s}^{-1}$  for the threshold angular frequency. This value is about one order of magnitude smaller than in Table I, showing the interest to be along a sweet line. For  $\nu \ll \omega_{th}$ , we again find that  $T_2$  behaves like  $2/\nu$  for reasons discussed in Sec. III of the Supplemental Material [46]. Beyond that, in the two-level model,  $T_2$  increases to reach values close to  $2T_1$ , and the dephasing process is limited by the spin relaxation. In the multilevel model, the high-frequency regime is once again influenced by coupling to higher-energy states. We thus find a behavior identical to the one obtained in the case where  $u_{\uparrow\uparrow} - u_{\downarrow\downarrow} \neq 0$ , but the value of  $\omega_{th}$  is here determined by the nondiagonal element of the perturbation Hamiltonian. However, it is interesting to note that, even if the nondiagonal term  $u_{\uparrow\downarrow}$  is responsible for the spin relaxation phenomenon, the value of  $T_2$  at frequency  $\omega_{th}$  [Eq. 14] is much lower than  $T_1$  [Eq. 10] at this same frequency:

$$T_1(\omega_{th}) = T_2(\omega_{th}) \frac{\hbar^2 \Omega^2}{2|u_{\uparrow\downarrow}|^2} \gg T_2(\omega_{th}). \quad (15)$$

The combined examination of Figs. 8(a) and 8(b) shows that it would be possible to select points along the lines  $u_{\uparrow\uparrow} - u_{\downarrow\downarrow} = 0$  where the values of  $|u_{\uparrow\downarrow}|$  and thus of  $\omega_{th}$  are even smaller, for example, by increasing the value of  $|V_{BG}|$ . In this case, the wave function of the hole is compressed against the side edges of the wire [44]. This increases confinement and hence splits  $E_1$  from the other energy levels, thus reducing the diagonal and nondiagonal coupling terms (Sec. II B of the Supplemental Material [46]). An alternative option to increase confinement would be to reduce the channel thickness and gate length, which is a real technological challenge given the already small dimensions of the current devices.

### B. Role of the direct Rashba effect

Several theoretical works have shown that hole bands in Si or Ge/Si nanowires can be characterized by a strong Rashba effect (called “direct”) under the action of an electric field [38,56,57]. This raises the question of the importance of this effect on spin decoherence in the qubit studied here. The Rashba interactions couple the spin to the momentum of the particle and can therefore bring additional dephasing while the dot is moving at finite speed following a change of state of the fluctuator. This process is naturally included in our time-dependent simulations of the multilevel model that describe the full dynamics of the wave function.

In the two-level model, the spin phase drift is induced by the succession of “quasistatic” configurations with different Larmor frequencies  $\Omega$  and  $\Omega'$ . Each configuration is characterized by stationary states given by the diagonalization of the  $2 \times 2$  matrices  $H_0$  and  $H_0 + U$ , respectively. So the phase decoherence results from the “deformation” of the wave function between the two configurations (as a rigid block displacement of the wave function does not change the Larmor frequency). We have seen previously that the two-level and multilevel models predict the same values of  $T_2$  for frequencies  $\nu$  of fluctuators below a certain threshold, as long as  $T_2 \ll T_1'$ . This

suggests that in this regime the “dynamic” effects and thus the direct Rashba effect do not influence  $T_2$ . It should also be noted that, still in this regime, we obtain almost unchanged values of  $T_2$  when we consider a modified telegraph signal in which the transitions  $0 \rightarrow 1$  and  $1 \rightarrow 0$  are no longer instantaneous but occur progressively (linearly) over a duration  $\Delta t$  of a few picoseconds, even though this duration is much longer than the tunnel time of the order of femtoseconds which is typically admitted (Appendix B). This demonstrates that the phase decoherence in the low-frequency regime does not depend on the dynamics of the transition between the two states.

It cannot be ruled out that the Rashba interactions contribute in the high-frequency regime for which two-level and multilevel models do not coincide. In this situation, the wave function is subject to very fast noise,  $\nu$  being much larger than the angular frequency  $\omega_{th}$ . However, the influence of the direct Rashba effect may be hidden by the fact that  $T_2$  is limited by  $T_1'$ , which highlights the complex dynamic effects due to the coupling with higher-energy states.

### C. Discussion of $T_1$

Our numerical simulations have shown that the relaxation time  $T_1$  obtained in a two-level model is not meaningful because the decoherence induced by the coupling to the highest-energy states, outside the doublet, is in fact faster with a characteristic time  $T_1'$ . However, this does not mean that the real  $T_1$ , the one that could be measured, is equal to  $T_1'$  for the following reasons.

The time  $T_1'$  reflects the fact that the weight of the hole wave function  $\psi(t)$  on the states beyond the fundamental doublet tends to grow with  $t$ , until a final situation where  $\psi(t)$  is statistically distributed on all the states of the considered basis (Sec. V of the Supplemental Material [46]). This evolution is very progressive,  $T_1'$  being very large compared with  $2/\nu$ , the average period of the telegraph signal. In our simulations, this evolution towards the final state is certain (statistically speaking) because the electronic system composed of the qubit and the fluctuator is not perturbed by any dissipative phenomenon. In fact, as the energy of the electronic system increases on average continuously, the probability that the system relaxes to a lower-energy state by coupling with a phonon or a photon should increase progressively. We can therefore deduce that multilevel simulations including electron-phonon coupling (or other dissipative phenomena) would be necessary to estimate  $T_1$  properly. It is highly unlikely that electron-phonon coupling will contribute to increase  $T_1$  relative to  $T_1'$  because the leakage of the hole state to states  $|\varphi_n^\alpha\rangle$  with  $n > 1$  is almost as effective with up ( $\alpha = \uparrow$ ) and down ( $\alpha = \downarrow$ ) spin states. So the question is whether this leakage will remain the dominant effect ( $T_1 \approx T_1'$ ) or whether the electron-phonon coupling will reduce  $T_1$ , which is obviously the case when phonon relaxation between  $\varphi_1^\uparrow$  and  $\varphi_1^\downarrow$  states becomes the dominant effect ( $T_1^{ph}$  is typically in the  $10^{-3}$ – $10^{-1}$  s range [37]). More generally, this raises very interesting questions about the cross influences between charge and spin relaxations in this system.

#### D. Comparison with experiments

It is now important to try to compare our simulation results with experimental data. In this section, we focus on Ref. [44], which reports on a four-gate device (gates G1–G4) fabricated from natural silicon. Remarkably, the authors of Ref. [44] are able to confine a single hole under gate G2, which allows a more direct comparison with the theoretical simulations.

Spin coherence measurements show the existence of very low frequency noise ( $10^{-4}$ – $10^{-2}$  Hz) probably induced by both hyperfine interactions and electrical fluctuations. Further measurements were therefore performed following a Hahn echo protocol that gets rid of the low-frequency noise sources. The echo amplitude follows a decay law in the form of a stretched exponential as a function of the waiting time (free evolution), representative of the high-frequency noise power spectrum ( $10^4$ – $10^6$  Hz). The characteristic time which is deduced, denoted as  $T_2^E$ , depends on the orientation of the magnetic field and reaches the remarkable value of 88  $\mu$ s at its maximum.

The authors of Ref. [44] clearly show that this high-frequency noise has an electrical origin. Let us assume that it comes from a very small number of fluctuators like those studied here. Each fluctuator  $n$  can be characterized by its threshold angular frequency  $\omega_{th}^n$  and by its oscillation frequency  $\nu_n$ . Let us also assume that each fluctuator remains in a non-Gaussian regime whatever the orientation of the magnetic field ( $\nu_n \ll \omega_{th}^n$ ). It is then easy to show that  $T_2^*$  is given by  $2/\sum_n \nu_n$  (Sec. III A of the Supplemental Material [46]), does not depend on the magnetic field orientation, and is not related to the noise spectrum  $S(\omega)$  for  $\omega \rightarrow 0$ . We can therefore deduce that the experimental system of Ref. [44] does not operate in this configuration.

The likely situation is that a significant part of the fluctuators involved in the measured noise are characterized by  $\nu_n > \omega_{th}^n$ , i.e., they operate in the Gaussian regime. As the measured time  $T_2^E$  is relatively long, this means that the threshold angular frequencies  $\omega_{th}^n$  are low, smaller than  $\approx 10^4$  Hz. Since  $\omega_{th} = |u_{\uparrow\uparrow} - u_{\downarrow\downarrow}|/\hbar$ , we conclude that the fluctuators involved are characterized by weak-coupling terms ( $U$  matrix), which corresponds to defects very far from the qubit, are characterized by a weak charge displacement ( $U \propto d$ , where  $d$  is the dipole), or have a dipole potential that is strongly screened, for example, by a hole gas [44]. This situation seems reasonable, the existence of far fluctuators being likely given the complex and immense environment around the qubit.

We cannot exclude that “non-Gaussian” fluctuators contribute to an isotropic noise background in Ref. [44]. It could be also interesting in the future to characterize noisier devices in order to see if non-Gaussian behaviors induced by a small number of “closer” telegraphic fluctuators can be highlighted. One could also imagine very low noise situations where the influence of the distant environment is reduced but remains influenced by a few extremely slow fluctuators for which  $\nu_n < \omega_{th}^n$ . In these cases, the dephasing time would become totally independent of the magnetic field orientation.

#### VI. CONCLUSION

We have simulated the spin decoherence in a hole qubit realized within a nanowire transistor in silicon-on-insulator technology. We consider the effect of a single fluctuating charge inducing telegraphic electrical noise. We show that the phase decoherence characterized by the time  $T_2$  is well described in a two-level model but in a non-Gaussian regime when the fluctuator operates at a frequency lower than a threshold value  $\omega_{th}$ . The simulations show that there are operating conditions of the component, along so-called “sweet” lines, for which  $\omega_{th}$  is shifted towards low frequencies, which results in an increase in the minimum value of  $T_2$ . However, this increase is limited due to the influence of nondiagonal coupling between the two states of opposite spin. For the spin relaxation characterized by the time  $T_1$ , we show on the other hand that a multilevel model is required, due to the coupling between the ground state of the hole and many higher-energy states. These results highlight a rich and relatively unexpected physics for a model problem with a single fluctuator perturbing the qubit. This shows the importance of quantum simulations including the most realistic description of the qubit. Our study should motivate future work on the subject, in particular using a multilevel description including electron-phonon coupling as a dissipative phenomenon.

#### ACKNOWLEDGMENT

This work was supported by the French National Research Agency (ANR project MAQSi, Project No. ANR-18-CE47-0007-02).

#### APPENDIX A: CALCULATION OF THE DECOHERENCE TIME $T_1'$

The characteristic time  $T_1'$  is defined to describe the leakage of the wave function of the hole out of the doublet composed of  $\varphi_1^\uparrow$  and  $\varphi_1^\downarrow$  states under the effect of the random variations of the perturbing potential. Our goal is to deduce  $T_1'$  from the evolution of  $\psi(t)$  obtained by solving the time-dependent Schrödinger equation, but we have to take into account two intrinsic limitations of this approach. First, a classical noise is considered while quantum effects can become important when  $kT$  is small compared with the energy gaps between levels. Second, dissipation effects are not included, for example, by coupling with phonons or by feedback to the fluctuator and the electron reservoirs. As a consequence, the long-time limit of  $\psi(t)$  cannot be physically correct in our model. Indeed, when the nondiagonal elements of the  $U$  matrix are zero, we show in Sec. V of the Supplemental Material [46] that the simulations will always converge to the situation where  $\psi(t)$  is statistically uniformly distributed over all the states of the system, which is to say that  $\langle |\langle \varphi_n^{\uparrow\downarrow} | \psi(t) \rangle|^2 \rangle_{\{E\}}$  converges to  $1/(2N)$  whatever  $N$  is, whereas it should tend to the value given by a quasi-Fermi-Dirac statistic if dissipative phenomena are taken into account.

As a consequence, we have limited our analysis to short times for which the quantity  $p_1(t) = \langle |\langle \varphi_1^\uparrow | \psi(t) \rangle|^2 +$

$|\langle \varphi_1^\downarrow | \psi(t) \rangle|^2 \rangle_{|E\rangle}$  has an exponential decay of the form  $\exp(-t/T_1')$ , where  $T_1'$  quickly becomes independent of the number of states considered in the basis. This approach is sufficient to describe the initial evolution of the wave function of the hole to the  $\varphi_n^\uparrow$  and  $\varphi_n^\downarrow$  states for  $n > 1$  and not its subsequent evolution.

In practice, we found the monoexponential character of  $p_1(t)$  when we consider the time span for which this quantity varies from 1 to 0.5, and we found that the value of  $T_1'$  is converged for  $N = 20$  [Fig. 5(a)]. This value can easily be understood since the matrix elements of  $U$  between the states  $\varphi_1^{\uparrow\downarrow}$  and  $\varphi_n^{\uparrow\downarrow}$  decrease sharply for increasing values of  $n > 1$  (Fig. 4).

## APPENDIX B: EFFECT OF NONINSTANTANEOUS TRANSITIONS

The telegraphic noise model assumes that the transitions between the two states of the fluctuator are instantaneous. Here we discuss the influence of noninstantaneous transitions and their realism.

We consider a modified telegraphic signal  $\chi'(t)$  in which the fluctuator is assumed to vary progressively (linearly) between states 0 and 1 over a time  $\Delta t = 7$  ps. Figure 10(b) shows that the characteristic times calculated using  $\chi'(t)$  behave as a function of  $\nu$  in the same way as for the original telegraph signal  $\chi(t)$ . At low frequencies,  $T_2$  remains given by  $2/\nu$ , and the dephasing time remains limited by the average switching time of the fluctuator. On the other hand,  $T_1'$  reaches higher values due to the fact that transitions to higher-energy hole states are less likely. However, the overall behavior remains the same.

The question is therefore whether a value  $\Delta t$  of 7 ps is realistic. This does not appear to be the case, as tunneling times are typically in the femtosecond range [58,59], as can be estimated with the expression  $\tau_T = d\sqrt{m}/(2U_b)$ , in which  $d$  is the length of the tunneling barrier ( $\approx 1$  nm),  $U_b$  is its height ( $\approx 2$  eV), and  $m$  is the carrier effective mass (approximately equal to the free-electron mass). The characteristic times calculated for  $\Delta t$  in the femtosecond range are those

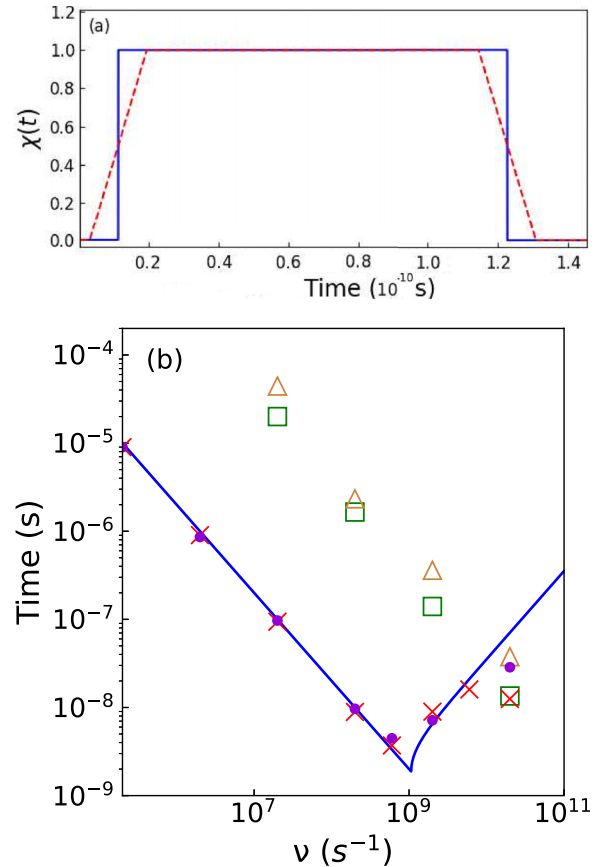


FIG. 10. (a) Modified telegraphic signal  $\chi'(t)$  in which the transition between states 0 and 1 is linear over a time  $\Delta t = 7$  ps (magenta dashed line), compared with the original telegraph signal  $\chi(t)$  (blue solid line). (b) Characteristic lifetimes  $T_1$  and  $T_2$  vs tunneling rate  $\nu$  calculated in the multilevel model ( $N = 10$ ) for trap 1. Green squares and brown triangles:  $T_1'$  calculated using  $\chi(t)$  or  $\chi'(t)$ , respectively. Red crosses and violet dots:  $T_2$  calculated using  $\chi(t)$  or  $\chi'(t)$ , respectively. The blue solid line depicts the analytical expression for  $T_2^*$ , as given by Eq. (8), using  $\omega_{th}$  and  $|u_{\uparrow\downarrow}|$  of Table I.

presented in Fig. 7. Therefore the instantaneous transitions model employed in this paper seems justified.

[1] B. Kane, A silicon-based nuclear spin quantum computer, *Nature (London)* **393**, 133 (1998).  
 [2] D. Loss and D. P. DiVincenzo, Quantum computation with quantum dots, *Phys. Rev. A* **57**, 120 (1998).  
 [3] J. J. Pla, K. Y. Tan, J. P. Dehollain, W. H. Lim, J. J. L. Morton, D. N. Jamieson, A. S. Dzurak, and A. Morello, A single-atom electron spin qubit in silicon, *Nature (London)* **489**, 541 (2012).  
 [4] F. A. Zwanenburg, A. S. Dzurak, A. Morello, M. Y. Simmons, L. C. L. Hollenberg, G. Klimeck, S. Rogge, S. N. Coppersmith, and M. A. Eriksson, Silicon quantum electronics, *Rev. Mod. Phys.* **85**, 961 (2013).  
 [5] E. Kawakami, P. Scarlino, D. R. Ward, F. R. Braakman, D. E. Savage, M. G. Lagally, M. Friesen, S. N. Coppersmith, M. A. Eriksson, and L. M. K. Vandersypen, Electrical con-

trol of a long-lived spin qubit in a Si/SiGe quantum dot, *Nat. Nanotechnol.* **9**, 666 (2014).  
 [6] M. Veldhorst, C. H. Yang, J. C. C. Hwang, W. Huang, J. P. Dehollain, J. T. Muhonen, S. Simmons, A. Laucht, F. E. Hudson, K. M. Itoh, A. Morello, and A. S. Dzurak, A two-qubit logic gate in silicon, *Nature (London)* **526**, 410 (2015).  
 [7] K. Takeda, J. Kamioka, T. Otsuka, J. Yoneda, T. Nakajima, M. R. Delbecq, S. Amaha, G. Allison, T. Kodera, S. Oda, and S. Tarucha, A fault-tolerant addressable spin qubit in a natural silicon quantum dot, *Sci. Adv.* **2**, e1600694 (2016).  
 [8] J. Yoneda, K. Takeda, T. Otsuka, T. Nakajima, M. R. Delbecq, G. Allison, T. Honda, T. Kodera, S. Oda, Y. Hoshi, N. Usami, K. M. Itoh, and S. Tarucha, A quantum-dot spin qubit with coherence limited by charge noise and fidelity higher than 99.9%, *Nat. Nanotechnol.* **13**, 102 (2018).

- [9] D. M. Zajac, A. J. Sigillito, M. Russ, F. Borjans, J. M. Taylor, G. Burkard, and J. R. Petta, Resonantly driven CNOT gate for electron spins, *Science* **359**, 439 (2018).
- [10] W. Huang, C. H. Yang, K. W. Chan, T. Tanttu, B. Hensen, R. C. C. Leon, M. A. Fogarty, J. C. C. Hwang, F. E. Hudson, K. M. Itoh, A. Morello, A. Laucht, and A. S. Dzurak, Fidelity benchmarks for two-qubit gates in silicon, *Nature (London)* **569**, 532 (2019).
- [11] A. M. Tyryshkin, S. Tojo, J. J. L. Morton, H. Riemann, N. V. Abrosimov, P. Becker, H.-J. Pohl, T. Schenkel, M. L. W. Thewalt, K. M. Itoh, and S. A. Lyon, Electron spin coherence exceeding seconds in high-purity silicon, *Nat. Mater.* **11**, 143 (2012).
- [12] M. Veldhorst, J. C. C. Hwang, C. H. Yang, A. W. Leenstra, B. de Ronde, J. P. Dehollain, J. T. Muhonen, F. E. Hudson, K. M. Itoh, A. Morello, and A. S. Dzurak, An addressable quantum dot qubit with fault-tolerant control-fidelity, *Nat. Nanotechnol.* **9**, 981 (2014).
- [13] A. Corna, L. Bourdet, R. Maurand, A. Crippa, D. Kotekar-Patil, H. Bohuslavskiy, R. Lavieville, L. Hutin, S. Barraud, X. Jehl, M. Vinet, S. De Franceschi, Y.-M. Niquet, and M. Sanquer, Electrically driven electron spin resonance mediated by spin-valley-orbit coupling in a silicon quantum dot, *npj Quantum Inf.* **4**, 6 (2018).
- [14] L. Bourdet and Y.-M. Niquet, All-electrical manipulation of silicon spin qubits with tunable spin-valley mixing, *Phys. Rev. B* **97**, 155433 (2018).
- [15] D. Bulaev and D. V. Loss, Spin Relaxation and Decoherence of Holes in Quantum Dots, *Phys. Rev. Lett.* **95**, 076805 (2005).
- [16] D. V. Bulaev and D. Loss, Electric Dipole Spin Resonance for Heavy Holes in Quantum Dots, *Phys. Rev. Lett.* **98**, 097202 (2007).
- [17] C. Kloeffel, M. Trif, P. Stano, and D. Loss, Circuit QED with hole-spin qubits in Ge/Si nanowire quantum dots, *Phys. Rev. B* **88**, 241405(R) (2013).
- [18] R. Li, F. E. Hudson, A. S. Dzurak, and A. R. Hamilton, Pauli spin blockade of heavy holes in a silicon double quantum dot, *Nano Lett.* **15**, 7314 (2015).
- [19] R. Maurand, X. Jehl, D. Kotekar-Patil, A. Corna, H. Bohuslavskiy, R. Lavieville, L. Hutin, S. Barraud, M. Vinet, M. Sanquer, and S. De Franceschi, A CMOS silicon spin qubit, *Nat. Commun.* **7**, 13575 (2016).
- [20] N. W. Hendrickx, W. I. L. Lawrie, L. Petit, A. Sammak, G. Scappucci, and M. Veldhorst, A single-hole spin qubit, *Nat. Commun.* **11**, 3478 (2020).
- [21] A. Crippa, R. Maurand, L. Bourdet, D. Kotekar-Patil, A. Amisse, X. Jehl, M. Sanquer, R. Lavieville, H. Bohuslavskiy, L. Hutin, S. Barraud, M. Vinet, Y.-M. Niquet, and S. De Franceschi, Electrical Spin Driving by  $g$ -Matrix Modulation in Spin-Orbit Qubits, *Phys. Rev. Lett.* **120**, 137702 (2018).
- [22] A. Crippa, R. Ezzouch, A. Apra, A. Amisse, R. Lavieville, L. Hutin, B. Bertrand, M. Vinet, M. Urdampilleta, T. Meunier, M. Sanquer, X. Jehl, R. Maurand, and S. De Franceschi, Gate-reflectometry dispersive readout and coherent control of a spin qubit in silicon, *Nat. Commun.* **10**, 2776 (2019).
- [23] H. Watzinger, J. Kukucka, L. Vukusic, F. Gao, T. Wang, F. Schaeffler, J.-J. Zhang, and G. Katsaros, A germanium hole spin qubit, *Nat. Commun.* **9**, 3902 (2018).
- [24] T. F. Watson, S. G. J. Philips, E. Kawakami, D. R. Ward, P. Scarlino, M. Veldhorst, D. E. Savage, M. G. Lagally, M. Friesen, S. N. Coppersmith, M. A. Eriksson, and L. M. K. Vandersypen, A programmable two-qubit quantum processor in silicon, *Nature (London)* **555**, 633 (2018).
- [25] X. Xue, T. F. Watson, J. Helsen, D. R. Ward, D. E. Savage, M. G. Lagally, S. N. Coppersmith, M. A. Eriksson, S. Wehner, and L. M. K. Vandersypen, Benchmarking Gate Fidelities in a Si/SiGe Two-Qubit Device, *Phys. Rev. X* **9**, 021011 (2019).
- [26] N. W. Hendrickx, D. P. Franke, A. Sammak, G. Scappucci, and M. Veldhorst, Fast two-qubit logic with holes in germanium, *Nature (London)* **577**, 487 (2020).
- [27] J. C. Abadillo-Uriel, C. King, S. N. Coppersmith, and M. Friesen, Long-range two-hybrid-qubit gates mediated by a microwave cavity with red sidebands, *Phys. Rev. A* **104**, 032612 (2021).
- [28] N. Holman, D. Rosenberg, D. Yost, J. L. Yoder, R. Das, W. D. Oliver, R. McDermott, and M. A. Eriksson, 3D integration and measurement of a semiconductor double quantum dot with a high-impedance TiN resonator, *npj Quantum Inf.* **7**, 137 (2021).
- [29] D. J. Ibberson, T. Lundberg, J. A. Haigh, L. Hutin, B. Bertrand, S. Barraud, C.-M. Lee, N. A. Stelmashenko, G. A. Oakes, L. Cochrane, J. W. A. Robinson, M. Vinet, M. F. Gonzalez-Zalba, and L. A. Ibberson, Large dispersive interaction between a CMOS double quantum dot and microwave photons, *PRX Quantum* **2**, 020315 (2021).
- [30] V. P. Michal, J. C. Abadillo-Uriel, S. Zihlmann, R. Maurand, Y. M. Niquet, and M. Filippone, Tunable hole spin-photon interaction based on  $g$ -matrix modulation, *Phys. Rev. B* **107**, L041303 (2023).
- [31] C. X. Yu, S. Zihlmann, J. C. Abadillo-Uriel, V. P. Michal, N. Rambal, H. Niebojewski, T. Bedecarrats, M. Vinet, É. Dumur, M. Filippone, B. Bertrand, S. De Franceschi, Y.-M. Niquet, and R. Maurand, Strong coupling between a photon and a hole spin in silicon, *Nat. Nanotechnol.* (2023).
- [32] S. Bosco, P. Scarlino, J. Klinovaja, and D. Loss, Fully Tunable Longitudinal Spin-Photon Interactions in Si and Ge Quantum Dots, *Phys. Rev. Lett.* **129**, 066801 (2022).
- [33] B. Martinez and Y.-M. Niquet, Variability of Electron and Hole Spin Qubits Due to Interface Roughness and Charge Traps, *Phys. Rev. Appl.* **17**, 024022 (2022).
- [34] D. Culcer, X. Hu, and S. Das Sarma, Dephasing of Si spin qubits due to charge noise, *Appl. Phys. Lett.* **95**, 073102 (2009).
- [35] A. Bermeister, D. Keith, and D. Culcer, Charge noise, spin-orbit coupling, and dephasing of single-spin qubits, *Appl. Phys. Lett.* **105**, 192102 (2014).
- [36] F. Maier, C. Kloeffel, and D. Loss, Tunable  $g$  factor and phonon-mediated hole spin relaxation in Ge/Si nanowire quantum dots, *Phys. Rev. B* **87**, 161305(R) (2013).
- [37] J. Li, B. Venitucci, and Y.-M. Niquet, Hole-phonon interactions in quantum dots: Effects of phonon confinement and encapsulation materials on spin-orbit qubits, *Phys. Rev. B* **102**, 075415 (2020).
- [38] C. Kloeffel, M. J. Rancic, and D. Loss, Direct Rashba spin-orbit interaction in Si and Ge nanowires with different growth directions, *Phys. Rev. B* **97**, 235422 (2018).
- [39] E. Paladino, Y. M. Galperin, G. Falci, and B. L. Altshuler,  $1/f$  noise: Implications for solid-state quantum information, *Rev. Mod. Phys.* **86**, 361 (2014).
- [40] B. Venitucci, L. Bourdet, D. Pouzada, and Y.-M. Niquet, Electrical manipulation of semiconductor spin qubits within the  $g$ -matrix formalism, *Phys. Rev. B* **98**, 155319 (2018).

- [41] B. Venitucci and Y.-M. Niquet, Simple model for electrical hole spin manipulation in semiconductor quantum dots: Impact of dot material and orientation, *Phys. Rev. B* **99**, 115317 (2019).
- [42] M. Benito, X. Croot, C. Adelsberger, S. Putz, X. Mi, J. R. Petta, and G. Burkard, Electric-field control and noise protection of the flopping-mode spin qubit, *Phys. Rev. B* **100**, 125430 (2019).
- [43] S. Bosco, B. Hetényi, and D. Loss, Hole Spin Qubits in Si FinFETs with fully tunable spin-orbit coupling and sweet spots for charge noise, *PRX Quantum* **2**, 010348 (2021).
- [44] N. Piot, B. Brun, V. Schmitt, S. Zihlmann, V. P. Michal, A. Apra, J. C. Abadillo-Uriel, X. Jehl, B. Bertrand, H. Niebojewski, L. Hutin, M. Vinet, M. Urdampilleta, T. Meunier, Y.-M. Niquet, R. Maurand, and S. De Franceschi, A single hole spin with enhanced coherence in natural silicon, *Nat. Nanotechnol.* **17**, 1072 (2022).
- [45] J. Bergli, Y. M. Galperin, and B. L. Altshuler, Decoherence in qubits due to low-frequency noise, *New J. Phys.* **11**, 025002 (2009).
- [46] See Supplemental Material at <http://link.aps.org/supplemental/10.1103/PhysRevB.107.125415> for details and additional results on the numerical calculations, on the dependence of the perturbation matrix elements with magnetic field, on the origin of the  $1/\nu$  law of the dephasing time  $T_2$ , on the  $g$  matrix of the hole qubit, on the long-time limit of a  $N$ -level system perturbed by a low-frequency telegraphic noise, on the energy levels and coupling strengths for the traps 2 and 3, on 2D maps of  $\Omega$  and  $u_{\uparrow\uparrow} - u_{\downarrow\downarrow}$ , and on  $m(t)$  at different frequencies  $\nu$ .
- [47] M. Graf and P. Vogl, Electromagnetic fields and dielectric response in empirical tight-binding theory, *Phys. Rev. B* **51**, 4940 (1995).
- [48] J. M. Luttinger, Quantum theory of cyclotron resonance in semiconductors: General theory, *Phys. Rev.* **102**, 1030 (1956).
- [49] B. S. Abel, Macroscopic superposition states and decoherence by quantum telegraph noise, Ph.D. thesis, Fakultät für Physik, Ludwig-Maximilians-Universität, 2008.
- [50] C. Leforestier, R. Bisseling, C. Cerjan, M. Feit, R. Friesner, A. Guldberg, A. Hammerich, G. Jolicard, W. Karrlein, H.-D. Meyer, N. Lipkin, O. Roncero, and R. Kosloff, A comparison of different propagation schemes for the time dependent Schrödinger equation, *J. Comput. Phys.* **94**, 59 (1991).
- [51] Y. M. Galperin, B. L. Altshuler, and D. V. Shantsev, Low-frequency noise as a source of dephasing of a qubit, in *Fundamental Problems of Mesoscopic Physics: Interactions and Decoherence*, edited by I. V. Lerner, B. L. Altshuler, and Y. Gefen (Springer, Dordrecht, 2004), pp. 141–165.
- [52] B. Abel and F. Marquardt, Decoherence by quantum telegraph noise: A numerical evaluation, *Phys. Rev. B* **78**, 201302(R) (2008).
- [53] A. A. Clerk, M. H. Devoret, S. M. Girvin, F. Marquardt, and R. J. Schoelkopf, Introduction to quantum noise, measurement, and amplification, *Rev. Mod. Phys.* **82**, 1155 (2010).
- [54] Z. Wang, E. Marcellina, A. R. Hamilton, J. H. Cullen, S. Rogge, J. Salfi, and D. Culcer, Optimal operation points for ultrafast, highly coherent Ge hole spin-orbit qubits, *npj Quantum Inf.* **7**, 54 (2021).
- [55] C. Adelsberger, M. Benito, S. Bosco, J. Klinovaja, and D. Loss, Hole-spin qubits in Ge nanowire quantum dots: Interplay of orbital magnetic field, strain, and growth direction, *Phys. Rev. B* **105**, 075308 (2022).
- [56] C. Kloeffel, M. Trif, and D. Loss, Strong spin-orbit interaction and helical hole states in Ge/Si nanowires, *Phys. Rev. B* **84**, 195314 (2011).
- [57] J.-W. Luo, S.-S. Li, and A. Zunger, Rapid Transition of the Hole Rashba Effect from Strong Field Dependence to Saturation in Semiconductor Nanowires, *Phys. Rev. Lett.* **119**, 126401 (2017).
- [58] R. Landauer and T. Martin, Barrier interaction time in tunneling, *Rev. Mod. Phys.* **66**, 217 (1994).
- [59] P. Février and J. Gabelli, Tunneling time probed by quantum shot noise, *Nat. Commun.* **9**, 4940 (2018).